Supported Nanometric Titanium Oxide Sols as a New Efficient Photocatalyst

M. Benmami, K. Chhor, and A. V. Kanaev*

Laboratoire d'Ingénierie des Matériaux et des Hautes Pressions, C.N.R.S., Institut Galilée, Université Paris-Nord, 93430 Villetaneuse, France

Received: March 17, 2005; In Final Form: August 17, 2005

We report on the first study of the photocatalytic performance of immobilized smallest titanium oxide oxoparticles of the size $2R = 5.0$ nm on a glass support. The nanometric particles are prepared in the sol−gel reactor with rapid reagent mixing and temperature, atmosphere, and particle size control. The surface coverage is achieved by inserting the support into the reactor solution during the induction period, where chemically active nanoparticles are relatively stable. We show that this immobilized amorphous oxo phase of titanium oxide exhibits considerable activity toward photocatalytic degradation of trichloroethylene in the gas phase. Moreover, one of the important factors appears to be the catalyst surface preparation, which has to be free of the adsorbed alcohol molecules. UV-assisted exchange between propoxy and hydroxy groups is suggested as the surface activation mechanism. The film thickness is expected to strongly affect the material photocatalytic efficiency because of the internal traps population.

I. Introduction

Photocatalytic applications require materials with a high density of electronic traps. A strong reason for that is the potential ability of separation and long-term conservation of photoinduced charges that are available for chemical reactions. In this sense, amorphous materials are particularly attractive because of the inherent disorder decreasing the free charge mobility and favoring trapping. Unfortunately, there are several major drawbacks. First, amorphous materials possess a grand density of the internal traps, whereas successful photocatalytic application requires surface traps, which are accessible by environmental pollutant molecules. Second, the traps often attract both charges, negatively charged electrons and a positively charged hole, resulting in their recombination.[1] Advantageously, bulk traps are almost absent in nanoparticles possessing a grand surface-to-volume ratio, where charges are mainly localized at the surface. However, free charges are confined in a small particle volume and their recombination dominates. This strongly decreases the charge separation efficiency and related material photocatalytic efficiency.

A solution to these problems could be found in the formulation of supported nanostructured materials, provided a particle−support interface induces preferential elimination of charge carriers of one sign from the particle. In this case, charge carriers of the opposite sign will undergo trapping at the particle surface. Such a function may be assured by Si−OH groups, which are produced on silica support by chemisorption of water molecules.[2] Additionally, supported nanoparticles are open structures with almost all the surface available for a contact with pollutant molecules. The relevant task would be to immobilize a thinnest monolayer of nanometric particles on an appropriate support.

One of prospective materials for supported nanophotocatalyst formulation is titanium oxide. It is widely used for both gas-phase and liquid-phase effluent depollution.[3−8] It also exhibits excellent bactericidal activity.[9] Moreover, it can be produced as nanometric particles suitable for immobilization on inorganic supports. A sol−gel process of transition metal alkoxides is a way to produce a nanometric sol of titanium oxide particles. Different experimental approaches and supports were considered for titanium oxide sol−gel thin films deposition.[10−15] Recently, a nanocoating using the sol−gel process has been considered as an approach for preparation of nanostructured materials.[16] However, suspended particles are generally considered as more photocatalytically active than immobilized ones.[17] Moreover, the crystalline anatase phase of titanium dioxide is considered for photocatalysis, whereas the amorphous phase is reported to be not active. Little progress in the understanding of photocatalytic properties of thinnest nanocoatings and, in particular, of the disordered amorphous phase, has been achieved up to now. However, the oxo phase is an interesting system as it possesses an extremely high charge trap density.[18] Moreover, chemical activity of the trapped electrons as Ti^{3+} centers has been recently demonstrated.[19] This suggests revising the general approach to this catalyst formulation.

Elaborated material control is an important point in studies of the photocatalytic performance of nanocoatings. A poor control of the process kinetics is an obstacle for successful preparation of monolayer of titanium oxide particles using the sol−gel method. Moreover, preparation of stable colloids by surfactant encapsulation is not appropriate for photocatalytic applications because it weakens particle contact with both support and pollutant. The posttreatment then would require removing the stabilizing shell, which can irreversibly affect the film structure. Recently, on the basis of our earlier kinetic studies[20−23] we have developed the sol−gel reactor with rapid reagent mixing and temperature, atmosphere, and particle size control.[24−26] This ensures process reproducibility in terms of kinetics. The sol particles of size $2R = 5.0$ nm in oxo phase have been prepared using titanium tetraisopropoxide, $Ti(OPr^i)_4$ (TTIP), as a precursor. This approach allowed revealing of important features of the sol build up kinetics and particle morphology during the induction time.[27] These sol nanoparticles are noncrystalline, possessing inorganic titanium oxide core and

* Corresponding author. E-mail: kanaev@limhp.univ-paris13.fr..

10.1021/jp051396+ CCC: $30.25
Published on Web 09/30/2005

surface propoxy and hydroxy groups. They exhibit high reactivity and are capable forming strong covalent bonding to substrate active sites.

We report on the first study of the photocatalytic performance of the immobilized smallest titanium oxide oxo-particles of $2R = 5.0$ nm on a glass support. The surface coverage is achieved by insertion of the support into the reactor solution during the induction period, where chemically active nanoparticles are relatively stable. We show that this immobilized precrystalline phase of titanium oxide exhibits considerable activity toward photocatalytic degradation of trichloroethylene, C_2HCl_3 (TCE), in the gas phase. Moreover, one of the important factors appears to be the surface preparation of the immobilized particles, which has to be free of the adsorbed alcohol molecules. The film thickness is expected to strongly affect the material photocatalytic efficiency because of the internal trap population.

II. Experiment

A. Preparation of Reactive Nanoparticles. Titanium oxide synthesis by the sol−gel process has been carried out in the reactor as described in refs 24−27. In short, two stock solutions, 50 cm^3 of a TTIP/propan-2-ol solution and 50 cm^3 of a H_2O/propan-2-ol solution, were injected into the reactor container through the static Hartridge−Roughton type T-mixer by applying dry nitrogen gas pressure through the synchronously opened magnetic valves with an opening time of several milliseconds. The TTIP concentration in the reactor solution was 0.146 M and the hydrolysis ratio $H = [H_2O]/[TTIP] = 2.46$. TTIP of 98% purity, propan-2-ol (Interchim), and distilled water were used in the experiments. In the experimental operating conditions, reagent micromixing occurred in the T-mixer within 2−5 ms, which is shorter than the characteristic time of primary hydrolysis−condensation reactions, resulting in nucleation. This allowed homogenizing the reactive mixture before the sol−gel process began and ensured almost δ-like nuclei size distribution. The temperature of the reactor solution of 20.00 ± 0.02 °C was controlled by a thermocryostat (Haake, DC10K15). A fiber optical probe was developed to monitor in situ the particle size ($2R$) and the scattered light intensity (I) of a He−Ne laser by the photon-correlated spectroscopy method, using a 16-bit, 255-channel PC board plugged digital correlator (PhotoCor Instruments) developed by Yudin et al.[28] The equipment allowed measuring of particles as small as $R \geq 1$ nm. The measurements (I, R) were carried out in the automatic sampling mode every 60 s. The use of this sol−gel reactor is an important point because it ensures the kinetics reproducibility and strongly reduces the experimental error bars.

The nucleation proceeded immediately during the reagent passage through the T-mixer. The particle size slowly increased during the induction period from 5.0 (nuclei) to ~10 nm. This was due to the particle aggregation process, as their total mass was conserved.[29] The induction period in the experimental conditions amounted to 53 ± 2 min. After this time, the colloid lost the stability and the sol particles precipitated.

B. Immobilization of Nanoparticles. The immobilization of reactive colloidal nanoparticles was achieved during the period of their relative stability, within the first half of the induction period. During this time, the support was introduced into the reactor solution. Colloidal nanoparticles are chemically very active. They react to the support active sites and remain at the surface. The support was then withdrawn from the reactor into a dry atmosphere. The liquid layer that covered the support surface could then be removed by flashing with liquid alcohol or by contact with absorbent paper. This is important in order to remove excessive nanoparticles that are not directly bound to the support. These particles tend to condense with time, increasing the layer thickness and contributing to the internal defects creation. We used small glass beads (spheres of 1-mm diameter) as supports. For simplicity, these wet spheres, after being in contact with the reactor colloid, were put on the adsorbent paper for several hours in the dry atmosphere until they became dry.

In the current experiments, we compared the photocatalytic activity of our prepared oxoparticles with that of Degussa P-25 TiO_2. This catalyst was supported on the 1-mm glass beads by using a simple coating method. The glass beads to be coated were first washed with 5M H_2SO_4 at 50 °C. An aqueous slurry containing 5% Degussa P-25 TiO_2 particles was used to coat the photocatalyst onto the glass beads, which were then fired at 450 °C for 4 h.

The mass of the catalyst used in this study was obtained from the procedure using an ammonium sulfate $(NH_4)_2SO_4$/sulfuric acid H_2SO_4 digestion.[30] The samples were added to the above mixture and carefully heated at 4 and 48 h, respectively, for oxo and Degussa P-25 TiO_2 films. The difference in these times is explained by the fact that the solubility of crystalline Degussa P-25 TiO_2 particles is considerably lower than that of the oxoparticles. The resulting solutions were filtered, diluted with distilled water, and complexed with H_2O_2 to form the orange solution. The determination of the titania concentration was performed using an UV−vis spectrometer (Cary 300, Varian). The average amount of Ti obtained for oxo and Degussa P-25 TiO_2 films were, respectively, 0.35 and >5.2 mg/g of the glass beads. The catalyst amounts obtained by weighing of the glass beads before and after the coating were in agreement with those determined previously.

C. Photocatalytic Reactor. The photocatalytic performance of the immobilized titanium oxide sols was studied by using the gas-phase continuous-flow reactor. Trichloroethylene (TCE) was used as a model pollutant[31−33] at concentrations ranging from 200 to 500 ppm, and a humid air at $p \approx 1$ bar was used as a carrier gas. The concentration of water vapor corresponded to an almost 10% relative humidity in the experimental conditions ($T = 20$ °C). The overall gas flow, measured by two mass flowmeters (Brooks) was about 250 cm^3/min. The gas mixture passed through two reactor tubes of either 6-mm or 10-mm internal diameter filled with glass beads, whose masses were correspondingly 7.5 g (2.6 mg of the oxocatalyst) and 24 g (8.4 mg). In experiments with the Degussa P-25 TiO_2 catalyst, its mass in the 6-mm reactor tube was >40 mg. The TCE pollutant residence times in the reactor were correspondingly 1.1 and 2.7 s. The reactor tubes were made of glass, transparent in the UV optical range above 320 nm. Six UV lamps (with the maximum intensity at 362 nm and $\Delta\lambda_{hwfm} = 22$ nm), each of 8 W power and 29 cm long, were positioned around the reactor tube at a 30-mm distance. The concentrations of the pollutant before and after the photocatalytic reactor were analyzed by a gas chromatograph (HP 5880 series) equipped with a capillary column (RTX 200) and a flame ionization detector FID. The reactor temperature was permanently monitored using the thermocouple K (chromel/alumel). Necessary tests were made to verify that no direct photolysis of TCE pollutant was observed in our experimental conditions.

III. Results and Discussion

A. Nanocoating Characterization. In the current study, we used as catalyst the titanium oxide particles in the oxo phase.

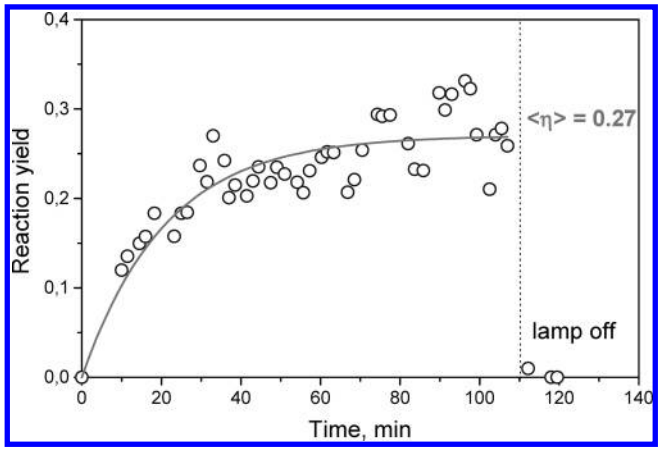

Figure 1. Photocatalytic performance of the coated spheres placed in the reactor of 6-mm tube diameter.

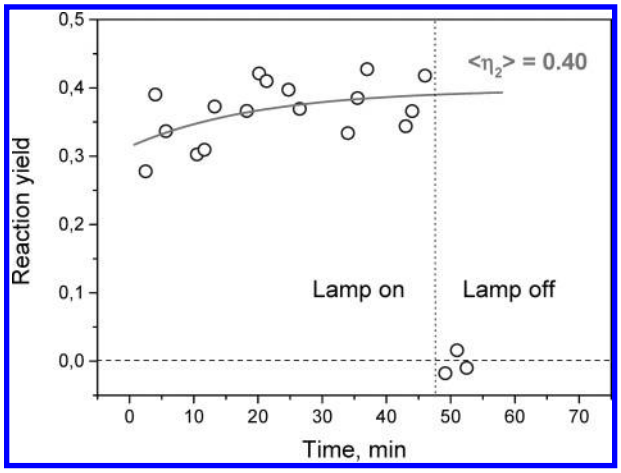

Figure 2. Photocatalytic performance of the coated spheres placed in the reactor of 10-mm tube diameter.

These particles are characterized by a general formula $TiO_a(OH)_b(OR)_{4-2a-b}$. Their formation is explained by the fact that the hydrolysis of the metal organic precursor TTIP is not complete even if a large excess of water ($H \gg 2$) is used.[34] These particles are essentially amorphous, as their building blocks are extremely chemically active clusters, such as $Ti_3O(OPr^i)_{10}$ or $Ti_{11}O_{13}(OPr^i)_{18}$,[35] which intermediate in the rapid nucleation process ($t \leq 0.1$ s in our conditions). The evaluation of the nuclei condensation ratio in our experimental conditions ($k = 1.45$ from ref 21) shows that the mean composition of an elementary unit is $TiO_{1.5}(X)$, which is explained by condensation of three titanium atom bonds, whereas the fourth one still processing the residual alkoxy or hydroxy groups is $X = OPr^i$, OH. Moreover, the immobilized particles have not been treated thermally. In these conditions, adsorbed alcohol molecules can also cover a considerable part of the particle surface.

The charge localization process in the sols may be similar to that in the gels, possessing a similar microcomposition. Between the gels, the colloidal and polymer forms are known.[36] We have recently observed that the charge separation and localization processes occur in these gel compounds with a high efficiency, which can exceed 20%.[18,19] Moreover, the relevant electrons trapped as Ti^{3+} centers possess an important chemical potential, which renders the photocatalytic process feasible.

We have obtained the deposited mass of 0.35 mg/g of glass spheres or 0.45 μg of the oxoparticles on one 1-mm sphere. This results in a thickness of the deposited layer of 36 ± 2 nm. This is an equivalent to $\sim$7 monolayers of the colloidal nanoparticles on the surface of one 1-mm sphere.

The specific area of the immobilized catalyst measured by BET method (Coulter SA3100) is 480 m^2/g, when normalized on the oxoparticles mass. This value is higher than that usually reported for such materials. The limit specific area of our titanium oxide particles, assuming their spherical shape, can be evaluated as $\bar{s} = 3/\rho R$. Estimating the oxoparticles density to be equal to $\sim$3.0 g/cm^3 (3/4 of the solid titanium oxide density, according to the unitary formula) we obtain $\bar{s} \approx 450$ m^2/g. This value is very close to that measured in our current experiments. This shows that the particles do not form the compact layered, but rather open structures on the glass sphere surface.

B. Photocatalytic Performance of Nanocoating. The photocatalytic performance of the immobilized oxoparticles is shown in Figure 1 and Figure 2. These two experiments were conducted in identical conditions in two reactor tubes, correspondingly of 6 mm and 10 mm diameters. The TCE pollutant concentrations before (p_{in}) and after (p_{out}) the reactor were measured, and the calculated reaction yield $\eta = (p_{in} - p_{out})/p_{in}$ is presented in these figures as a function of time. All tested immobilized oxocatalysts fabricated by the above-described method have shown photocatalytic activity toward TCE degradation. Two main features of these kinetic curves are (i) the initial transient period and (ii) stationary achieved at long irradiation times. The long-term material performance has not been studied. However, during the two-hour continuous irradiation period, no decrease of the reactor performance has been observed. Additionally, the material exhibits a stable performance when reused with a delay of days. We discuss below these features in more detail.

We have observed that at the beginning of the process the reaction yield is almost zero and it slowly increases with time. However, this effect appeared to be sensitive to the time period the catalyst is flashed with the dry carrier gas before the lamp is switched on. In the experiments discussed in Figures 1 and 2, this time was approximately 2 and 4 h correspondingly and the initial reaction yield amounts for 30% and 80%, respectively, of the maximum value attained at $t \rightarrow \infty$. The observed effect is not related to the reactor temperature. Indeed, the temperature of the reactor is found to increase from a room one of $\sim$23−38 °C during first 50 min of the work (see Figure 3b). However, if the flashing time is long (more than 6 h in Figure 3a), the transient period was almost absent. Moreover, once the catalyst is activated to the maximum value, its performance remains stable even after interruption of the experiment for days. We conclude that the effect is related to the particle surface preparation.

To understand this effect, we have carried out DSC-ATG (Setaram) measurements of the particle mass loss at heating. The curve presented in Figure 4 has been obtained with a scanning rate of 2.0 °C/min. These results indicate that the oxoparticles lose about 34% of their mass, which may belong to adsorbed alcohol and water molecules and residual nonhydrolyzed alkoxy groups, −OR of titania. This process is almost completed below 400 °C, when a crystalline anatase phase is formed. This last conclusion is confirmed by appearance of a strong exothermic peak on a heat flux curve. In the lower temperature domain, two strong features exist, at about 205 °C and below 100 °C. The first one is apparently related to the residual organics removal, as the particles become slightly brown and this is accompanied by a release of a heat. On the other hand, the broad feature below 100 °C can be identified to the adsorbed propan-2-ol molecules desorption from the particle surface. This is confirmed by the endothermic nature of the process and by the fact that no visible changes in the particles'

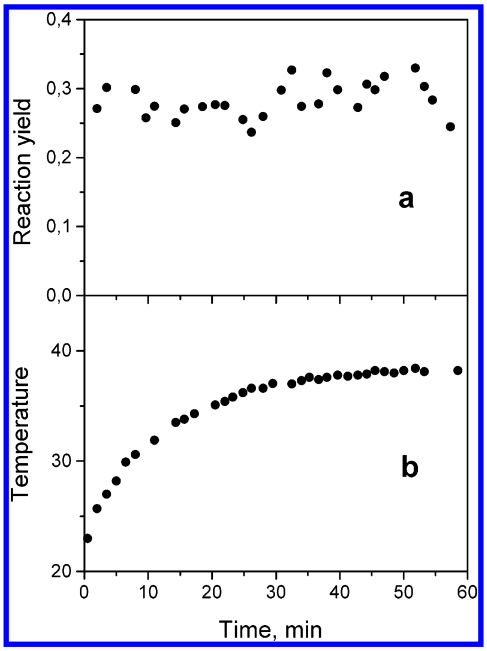

Figure 3. Photocatalytic performance of the coated spheres placed in the reactor of 6-mm tube diameter (a) and the reactor temperature (b).

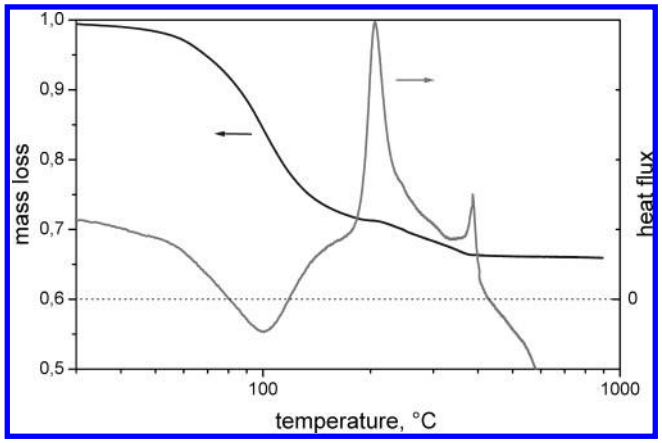

Figure 4. DSC-TGA analysis of the precipitated nanoparticles.

color have appeared. Particles lose almost 20% of their mass at this point. We conclude that the alcohol molecules cover almost all surfaces of the immobilized oxoparticles despite the prolonged drying at room temperature.

The particle surface covered by alcohol molecules is not active in photocatalysis, as our results show. However, continuous flashing by gas improves the catalyst performance. Apparently, this is related to the exchange reaction with water molecules added to the carrier gas. Moreover, as our experiments show, this effect is strongly accelerated at the UV irradiation, and less than 1 h is required to reach the stationary performance of the catalyst. We propose that a surface cleaning from alkoxy groups is responsible for this observation:

$$\ldots -\mathrm{Ti}-\mathrm{OR} + \mathrm{H_2O} + h\nu(3.42\ \mathrm{eV}) \xrightarrow{\text{gas flow}} \ldots -\mathrm{Ti}-\mathrm{OH} + \mathrm{ROH}$$

We remark that the immobilized amorphous oxoparticles cannot be transformed into crystalline TiO_2 because this process requires a much higher temperature than that attained in our photocatalytic reactor ($T_R \leq 40$ °C, see Figure 3b).

As it is known, molecules adsorb on the particle surface in two forms: molecular (physisorption) and dissociated into

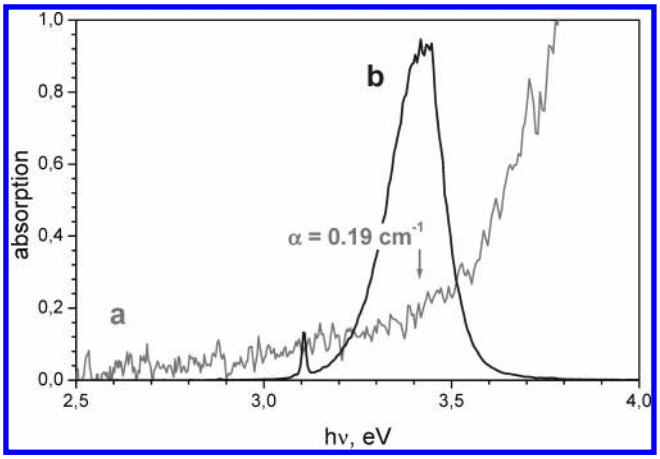

Figure 5. Absorption spectrum of the nanocoating on glass spheres (a) and the emission spectrum of the UV lamp (b).

fragments (chemisorption). The last one requires higher energy to be delivered. For example, methanol molecule adsorption free energy on a TiO_2 surface is 0.82 eV, whereas chemisorption entropy of methoxy is much higher, 2.52 eV.[37] The sites occupied by alkoxy groups are then active by nature and are supposed to be responsible for photocatalytic activity of titanium oxide particles. In contrast, alcohol molecules in the molecular form adsorbed on inactive surface sites. Physisorbed methanol in a molecular form as observed is much less sensitive to UV radiation. A related effect produced by UV irradiation on TiO_2 is observed as a surface wettability conversion.[38] Future analysis of surface exchange between alkoxy and hydroxy groups under UV (362 nm) irradiation is required to verify our hypothesis.

A simple model may represent the surface cleaning according to a first-order mechanism. We suppose S_0 and S to be the maximal possible and real active surfaces of the catalyst particles and Φ to be the flow of photons from the UV lamp. The equation is then

$$\frac{dS}{dt} = k\Phi\cdot(S_0 - S) \qquad (1)$$

where k is the constant. The solution of the eq 1 is

$$S = S_0(1 - \exp(-t/\tau)) \qquad (2)$$

with $\tau = (k\Phi)^{-1}$. Assuming that the reactions yield $\eta(t) \propto S(t)$, we have successfully treated the experimental data with eq 2 to obtain the stationary values of the reaction yields: $\eta^{(1)} = 0.27 \pm 0.02$ (6-mm reactor tube, see Figures 1 and 3) and $\eta^{(2)} = 0.40 \pm 0.02$ (10-mm reactor tube, see Figure 2). The effective transient time constant is $\tau = 20 \pm 3$ min.

Characterization of the nanocoating efficiency in photocatalysis requires knowledge of the material absorption. We have carried out a test of the transmission of the coated spheres placed in the 1.0-cm optical cell. In these experiments, the irradiation source (output of the 1-mm optical fiber coupled to the D_2 lamp) and the reception device (input of another 1-mm optical fiber coupled to the CCD spectrometer) were aligned in contact with the cell faces. The lamp intensity was attenuated in the cell because of two factors: material absorption (α) and light scattering (β). Our measurements show that the scattering processes dominate ($\beta \gg \alpha$). The absorption spectrum has been obtained in these conditions as a difference spectrum between that of coated and noncoated spheres. This spectrum is shown in Figure 5. along with the spectrum of the UV lamp used in the photocatalytic reactor. Because of a thin layer, the resulting

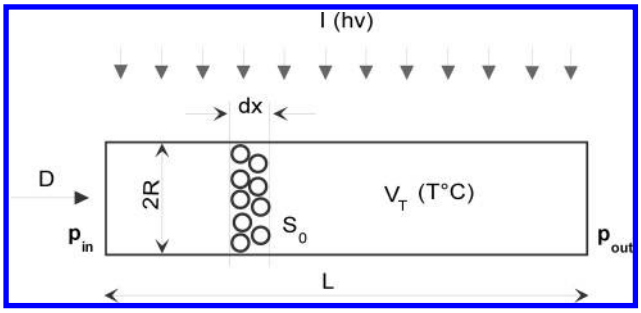

Figure 6. Reactor modeling: p, pollutant concentration before (in) and after (out) the reactor; D, gas debit of the gas; 2*R*, internal diameter of the reactor; I, lamp intensity (photons/cm^2); V_T, thermal velocity of pollutant molecules; S_0, total active surface of the catalyst.

material absorbance is very low and attains $\alpha = 0.19$ cm^{-1} at the wavelength of maximum intensity of the UV lamp (362 nm). This value as well as the condition $\beta \gg \alpha$ will be taken into account below to compare the photocatalytic efficiency of the oxoparticles with that of the spheres coated by Degussa P-25 TiO_2 powder. This last powder is a usual high-performance immobilized catalyst constituted of coagulated particles (~30 nm) of mixed anatase−amorphous and anatase−rutile polymorphs. Our measurements show that the deposited mass was in this case considerably larger than that of our oxoparticles. The solubility method resulted in >5.2 mg/g of glass spheres, or 6.7 μg of the Degussa P-25 TiO_2 particles on one 1-mm sphere, which is 15 times higher than in our prepared oxonanocoatings. This results in a thickness of the deposited layer of almost 0.54 μm. The photocatalytic test has shown the reaction yield of supported Degussa P-25 TiO_2 particles to be $\eta_0^{(D)} = 0.85$ (6-mm reactor tube of 2.5-cm length).

The comparison of the catalysts' performances will be performed on the basis of a simple model described below and explained in Figure 6. The gas containing the pollutant molecules at concentration p enters the reactor tube at the debit D, which corresponds to the velocity of $v = D/\pi R^2$. The pollutant molecules flow on the catalyst surface is expressed as $f = pV_T t/4$, where V_T stands for their thermal velocity ($V_T \gg v$) and t for the contact time. On impact with the surface, the reaction occurs with the efficiency γ, and s stands for the available catalyst surface of the unitary reactor volume in the stationary regime. However, the specific active surface s_a (averaged over the reactor cross section) can be obtained by a balance between the rates of UV photon absorption (α) and that of charge-transfer reactions. Assuming s_a is considerably lower than s, we can write:

$$s_a = s \cdot A(2\pi R/\pi R^2) I\tau_r = 2AsI\tau_r/R \qquad (3)$$

where A is the UV light absorption in the reactor volume, τ_r is the active center lifetime, and I is the lamp intensity at the reactor tube surface. One has to remark that, even when only the outer layers of the reactor are activated by light, strong gas mixing on flow through the compacted spheres rapidly homogenizes the pollutant concentration in the reactor cross section, which ensures its permanent contact with the activated catalyst and its decay. In the conditions of a high reactor transparency, $A \approx 2\alpha R$ and s_a in eq 3 does not depends on the tube radius R. However, in our case, because of a strong scattering, the light penetrates weakly into the reactor volume and s_a decreases with R. One can now obtain the expression for evolution of the pollutant concentration when passing a distance dx along the reactor tube:

$$\frac{dp}{dx} = -f\gamma s_a t = -\frac{\gamma}{4} pV_T \cdot \frac{2AsI\tau_r}{R} \cdot \frac{dx}{D} \pi R^2 \qquad (4)$$

(the contact time is taken here $t = dx/v$). We finally obtain

$$\frac{dp}{dx} = -\frac{\pi A\gamma V_T sI\tau_r R}{2D} \cdot p \qquad (5)$$

The solution of eq 5 is

$$p = p_0 \cdot \exp\left(-\frac{\pi A\gamma V_T sI\tau_r R}{2D} x\right) \qquad (6)$$

and the reaction yield can then be expressed as

$$\eta = 1 - \exp\left(-\frac{\pi A\gamma V_T sI\tau_r R}{2D} L\right) \qquad (7)$$

First, for sufficiently small η, eq 7 can be expressed as

$$\eta \approx \frac{\pi A\gamma V_T sI\tau_r R}{2D} L \qquad (8)$$

This equation describes the scaling law; when increasing the reactor tube diameter, $\eta/R = $ const. Our results obtained with the same immobilized catalyst in two reactor tubes of 6-mm and 10-mm diameter, $\eta^{(2)}/\eta^{(1)} \approx 1.5$, are in a good agreement with the radii ratio, $R^{(2)}/R^{(1)} \approx 1.6$.

By using eq 7, we can now compare photocatalytic activities of the immobilized oxoparticles with that of supported Degussa P-25 TiO_2 powder. Their measured stationary reaction yields are $\eta_0^{(D)} = 0.85$ and $\eta^{(1)} = 0.27$, respectively. From eqs 7−8, we can obtain

$$\frac{\pi A\gamma V_T sI\tau_r R}{2D} L = 0.24 \text{ and } 0.12 \qquad (9)$$

for Degussa P-25 TiO_2 and oxocatalysts, correspondingly. As we have already stated, the UV light is completely absorbed by the Degussa P-25 TiO_2 catalyst ($A_D \approx 1$), while the absorbance of the oxocatalyst is low. For the reactor tube diameter of 6 mm, this absorbance can be roughly estimated as $A_1 \approx 0.043$. Keeping in mind these values, we obtain from eq 9 the photocatalyst's efficiency ratio

$$\gamma_{oxo}/\gamma_{P25} \approx 0.3 \qquad (10)$$

The efficiency of this noncrystalline titanium oxide nanocoating appears to be comparable to that of one of the best Degussa P-25 TiO_2 photocatalysts. Moreover, our experimental results show that the reaction yield almost does not depend on the nanocoating thickness when it decreases. In the limit of the monolayer 5.0-nm particle coating, the compensated photocatalytic yield γ_{oxo} becomes higher than that of the Degussa P-25 TiO_2 photocatalyst.[39]

The high internal efficiency of the sol−gel nanocoatings is attributed by us to a high density of the electronic traps inherent to an amorphous-like oxo phase of titanium oxide[18,19] and to an extremely small size of the immobilized nanoparticles, which are arranged in almost open structures. A high surface-to-volume ratio of nanoparticles almost excludes the appearance of bulk traps, which are inefficient in photocatalysis. Moreover, the charge separation efficiency in our immobilized nanoparticles may be high. This is surprising, as structural imperfections of the amorphous phase of titanium dioxide, facilitating e^--h^+ recombination, are supposed to be responsible for its negligible

photocatalytic activity.[1] Because of this, only crystalline TiO_2 has been considered for applications in photocatalysis.[1,10,15,40,41] We assume that the support plays a major role in the charge separation process. This physics, as well as the nature of surface binding, and possible structural changes of the immobilized oxoparticles on the surface have to be elucidated in future studies.

The reported results show an interesting new nanocoating photocatalyst prepared by the sol−gel method. (i) The internal efficiency of the nanocoatings is at least as high as that of the best crystalline photocatalyst. (ii) Because of a very large specific surface area, a very low catalyst mass can be loaded in the reactors. (iii) The particles of nanocoatings are strongly bound to the support. This explains a considerably higher mechanical stability of our nanocoatings compared to that of the deposited TiO_2 powder. (iv) A low photoabsorption inherent to one nanocoating cannot be considered as a disadvantage, while a sufficient number of thin coatings can efficiently absorb UV light, e.g., larger reactor volumes may be illuminated in these conditions. (v) Our preparation excludes the calcination process, required for crystallization of the anatase TiO_2. This can be applied to protect substrates that does not allow thermal treatment because of their low thermal stability.

Although we have not demonstrated in this work the nanocoatings of the limit thickness ($\delta \approx 36$ nm has been obtained against expected 5 nm), future developments will certainly allow it. We believe that a decrease of the layer thickness is a way to increase the nanocoating efficiency in photocatalysis, as it reduces the internal trap density.

IV. Conclusion

We report on the first study of the photocatalytic performance of immobilized smallest titanium oxide oxoparticles. The nanometric particles of size $2R = 5.0$ nm are prepared by the sol−gel method in the reactor with rapid reagent mixing and temperature, atmosphere, and particle size control. The complex shape of the support (spherical glass beads) required an adequate method of particle deposition. Their immobilization is achieved by the insertion of the support into the reactor solution during the induction period, where chemically active nanoparticles are relatively stable. The oxoparticles react with available active sites and bind themselves to the surface. We show that this immobilized amorphous oxo phase of titanium oxide exhibits considerable activity toward photocatalytic degradation of the TCE pollutant in gas phase. The efficiency of the prepared nanocatalyst is similar to that of the best-known one, Degussa P-25 TiO_2. Moreover, one of the important factors appears to be the catalyst surface preparation, which has to be free of the adsorbed alcohol molecules. The film thickness is expected to strongly affect the material photocatalytic efficiency because of the internal trap population.

The obtained results suggest a new approach to the active component design, while the sol particles are not in one of the known crystalline polymorphs. Earlier, the anatase phase of titanium oxide was considered as the most efficient in photocatalysis, while the amorphous phase was reported to be inactive.

Acknowledgment. This work is supported by the COST D19 Action of the European Commission.

References and Notes

(1) Ohtani, B.; Ogawa, Y.; Nishimoto, S. *J. Phys. Chem. B* **1997**, *101*, 3746.

(2) Yates, J. T. *Surf. Sci.* **2004**, *565*, 103.

(3) Fujishima, A.; Honda, K. *Nature* **1972**, *37*, 238.

(4) *Photocatalysis: Fundamentals and Applications*; Serpone, N., Pelizzetti E., Eds.; Wiley: New York, 1989.

(5) Fujishima, A.; Rao, T. N.; Tryk, D. A. *J. Photochem. Photobiol., C: Photochem. Rev.* **2000**, *1*, 1.

(6) Linsebigler, A. L.; Lu, G.; Yates J. T., Jr. *Chem. Rev.* **1995**, *95*, 735.

(7) Hoffmann, M. R.; Martin, S. T.; Choi, W.; Bahnemann, D. W. *Chem. Rev.* **1995**, *95*, 69.

(8) *Photocatalytic Purification and Treatment of Water and Air*; Ollis, D. F., Al-Ekabi H., Eds.; Elsevier: Amsterdam, 1993.

(9) Lu, Z.-X.; Zhou, L.; Zhang, Z.-L.; Shi, W.-L.; Xie, Z.-X.; Xie, H.-Y.; Pang, D.-W.; Shen, P. *Langmuir* **2003**, *19*, 8765.

(10) Robert, D.; Piscopo, A.; Heintz, O.; Weber, J. V.; *Catal. Today* **1999**, *54*, 291.

(11) Chen, G.; Luo, G.; Yang, X.; Sun, Y.; Wang, J. *Mater. Sci. Eng., A* **2004**, *380*, 320.

(12) Danion, A.; Disdier, J.; Guillard, C.; Abdelmalekc, F.; Jaffrezic-Renaulta, N. *Appl. Catal., B* **2004**, *52*, 213.

(13) Martyanov I. N.; Klabunde, K. J. *J. Catal.* **2004**, *225*, 408.

(14) Bhattacharyya, A.; Kawi, S.; Ray, M. B.; *Catal. Today* **2004**, in press.

(15) Su, C.; Hong, B.-Y.; Tseng, C.-M.; *Catal. Today* **2004**, *96*, 119.

(16) Caruso R. A.; Antonietti, M.; *Chem. Mater.* **2001**, *13*, 3272.

(17) Xu, Y.; Langford, C. H. *J. Phys. Chem. B* **1997**, *101*, 3115.

(18) Kuznetsov, A.; Kameneva, O.; Alexandrov, A.; Bityurin, N.; Sanchez, C.; Chhor, K.; Marteau, Ph.; Kanaev, A. *Phys. Rev. E* **2005**, *71*, 21403.

(19) Kuznetsov, A.; Kameneva, O.; Alexandrov, A.; Bityurin, N.; Chhor, K.; Kanaev, A. *Chemical Activity of Photoinduced Ti^{3+} Centers in Titanium Oxide Gels*, **2005**, to be published.

(20) Monticone, S.; Soloviev, A.; Tufeu, R.; Kanaev, A. V. *AIDIC Conf. Ser.* **1999**, *4*, 77.

(21) Soloviev, A.; Tufue, R.; Sanchez, C.; Kanaev, A. *J. Phys. Chem. B* **2001**, *105*, 4175.

(22) Soloviev, A. Ph.D. Thesis, University Paris 13, France, 2000.

(23) Soloviev, A.; Jensen, H.; Søgaard, E. G.; Kanaev, A. V. *J. Mater. Sci.* **2003**, *38*, 3315.

(24) Rivallin, M.; Zeghlache, A.; Soloviev, A.; Gaunand, A.; Kanaev, A. *Chem. Eng. Trans.* **2002**, *1*, 969.

(25) Rivallin, M.; Benmami, M.; Kanaev, A.; Gaunand, A. *Chem. Eng. Res. Des.* **2005**, *83* (A1), 1.

(26) Rivallin, M. Ph.D. Thesis, ENSMP, France, 2000.

(27) Rivallin, M.; Benmami, M.; Gaunand, A.; Kanaev, A. *Chem. Phys. Lett.* **2004**, *398*, 157.

(28) Yudin, I. K.; Nilolaenko, G. L.; Kosov, V. I.; Agayan, V. A.; Anisimov, M. A.; Sengers, J. V. *Int. J. Thermophys.* **1997**, *15*, 1237.

(29) Soloviev, A.; Tufeu, R.; Sanchez, C.; Kanaev, A. *J. Phys. Chem. B* **2001**, *105*, 4175.

(30) Coronado, J. M.; Zorn, J. M.; Tejedor-Tejedor, I.; Anderson, M. *Appl. Catal., B* **2003**, *43*, 329.

(31) Hegedüs, M.; Dombi, A. *Appl. Catal., A* **2004**, *271*, 177.

(32) Amama, P. B.; Itoh, K.; Murabayashi, M. *J. Mol. Catal., A* **2004**, *217*, 109.

(33) Son, H.-S.; Lee, S.-J.; Cho, I.-H.; Zoh, K.-D. *Chemosphere* **2004**, *57*, 309.

(34) Blanchard, J.; Barboux-Doeuff, S.; Maquet, J.; Sanchez, C. *New J. Chem.* **1995**, *19*, 929.

(35) Sanchez, C.; Ribot, F. *New J. Chem.* **1994**, *18*, 1007.

(36) Pierre, A. C. *Introduction to Sol−Gel Processing*; Kluwer International Series in Sol−Gel Processing: Technology and Applications; Kluwer: Norwell, MA, 1998.

(37) Wang, C.; Groenzin, H.; Schultz, M. J. *J. Phys. Chem. B* **2004**, *108*, 265.

(38) Wang, R.; Sakai, N.; Fujishima, A.; Watanabe, T.; Hashimoto, K. *J. Phys. Chem. B* **1999**, *103*, 2188.

(39) Benmami, M.; Chhor, K.; Kanaev, A. To be published.

(40) Guillard, C.; Beaugiraud, B.; Dutriez, C.; Herrmann, J.-M.; Jaffrezic, H.; Jaffrezic-Renault, N.; Lacroix, M. *Appl. Catal., B* **2002**, *39*, 331.

(41) Tanaka, K.; Capule, M. F. V.; Hisanaga, T. *Chem. Phys. Lett.* **1991**, *187*, 73.